

A Simple Equivalent Circuit Model for Ultrawideband Coupled Arrays

Elias A. Alwan, *Student Member, IEEE*, Kubilay Sertel, *Senior Member, IEEE*, and John L. Volakis, *Fellow, IEEE*

Abstract—Equivalent circuits are proposed to model the radiation impedance of low-profile ultrawideband antenna arrays with strong interelement coupling. Previous approaches provided rudimentary equivalent circuits and referred to much smaller impedance bandwidth arrays. In this letter, we extend these models to include antenna sections that overlap with adjacent array elements (as is the case with interwoven arms of tightly coupled spirals). The proposed equivalent circuits include dielectric superstrates and representations of higher-order grating lobes. Design optimization is carried out for an array of coupled and interwoven antenna elements to develop a 20:1 impedance bandwidth aperture. It is demonstrated that the radiation impedance obtained via the proposed equivalent circuit is in excellent agreement with full-wave simulation.

Index Terms—Equivalent circuit, grating lobes, spiral antenna, ultrawideband antenna arrays.

I. INTRODUCTION

LOW-PROFILE arrays are highly desired for inconspicuous conformal integration in a wide range of situations. In terms of impedance bandwidth, popular wideband elements are tapered slots [1], which include Vivaldi-like antennas [2], TEM horns [3], and bunny-ear arrays [4]. Although these elements can realize wide bandwidths, they are nonplanar in nature. Furthermore, for low-frequency applications, such antennas tend to be large and protrusive (several wavelengths thick in profile).

Another class of wideband arrays, based on Wheeler's current sheet model [5], are planar by design. In particular, connected dipole [6] and long slot arrays [7] can exhibit large impedance bandwidth in freestanding operation. However, when conformally mounted on a platform [i.e., with a ground plane (GP) behind them], they suffer from GP shorting, severely limiting low-frequency operation. To overcome the GP interference, interelement mutual coupling was proposed by Munk [8]. Using this approach, a new class of low-cost, low-profile, ultrawideband (UWB) planar phased arrays was introduced to realize Wheeler's concept [5]. Specifically, an array of tightly coupled

Manuscript received December 05, 2011; revised January 03, 2012; accepted January 08, 2012. Date of publication January 13, 2012; date of current version March 19, 2012. This work was supported by the Office of Naval Research (ONR) under Grant N00014-11-0077.

The authors are with the ElectroScience Laboratory, The Ohio State University, Columbus, OH 43212 USA (e-mail: alwan.2@osu.edu; sertel.1@osu.edu; volakis@ece.osu.edu).

Color versions of one or more of the figures in this letter are available online at <http://ieeexplore.ieee.org>.

Digital Object Identifier 10.1109/LAWP.2012.2184257

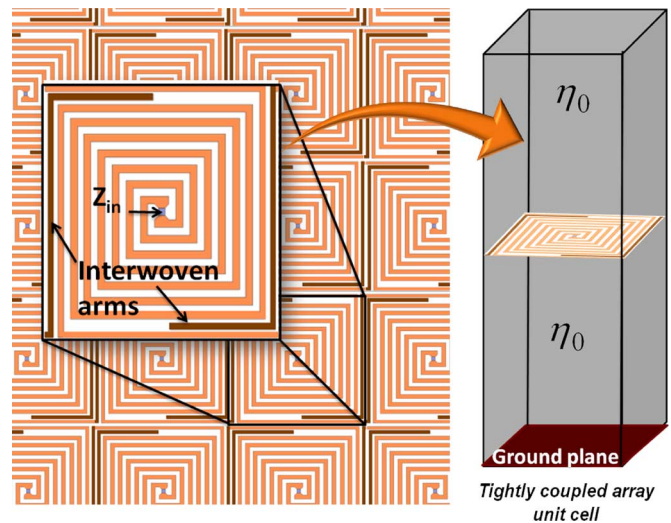


Fig. 1. Tightly coupled spiral array with interwoven arms.

dipoles with interdigital capacitors achieved an impressive 4.5:1 impedance bandwidth with the GP placed $\lambda_0/3$ (at the highest frequency) away from the aperture.

The “fragmented aperture” is another conformal UWB array based on numerical optimization of materials and geometry [9]. An impressive impedance bandwidth of 33:1 was reported in an infinite array setting. However, because of the material used and complex geometry, this array is difficult to realize. It also employs resistive cards, making it lossy.

The fragmented array [9] and the interwoven spiral by Tzanidis *et al.* [10] indicate that suitable array design with highly coupled elements can deliver much higher impedance bandwidths. However, full-wave computations are time-consuming for such an optimization. In this letter, we introduce a simple circuit model for designing tightly coupled arrays with a goal of achieving large, more than 10:1, impedance bandwidths. The model consists of transmission lines (TLs) and a combination of lumped elements (resistors, capacitors, and inductors) [8].

In this letter, this model is first used to verify the design of 10:1 interwoven planar spiral array presented in [10] (see Fig. 1). Then, we proceed to use this circuit to design a new interwoven spiral array having 20:1 impedance bandwidth with $VSWR < 3$. An important aspect of the proposed circuit model is the inclusion of higher-order modes supported by the transmission lines. This is important as the higher modes impact array impedance.

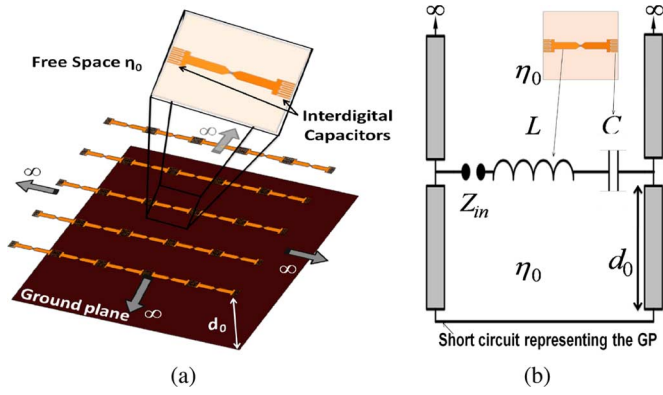


Fig. 2. (a) Munk's current sheet array over a ground plane with (b) the equivalent circuit to the right.

II. EQUIVALENT CIRCUIT FOR INTERWOVEN SPIRAL ARRAYS

The concept of using equivalent circuits to represent dipole-based antenna arrays was first demonstrated in [8]. This model is depicted in Fig. 2. We note from Fig. 2(b), that in addition to the dipole's self-inductance L , capacitive coupling between the dipole tips is included using lumped capacitors. Furthermore, the radiation resistance is included by introducing an infinite TL having a characteristic impedance of $\eta_0 = 377 \Omega$ [5]. The ground plane is also represented by a shorted TL. The length of the shorted transmission line is, of course, equal to the array thickness d_0 (i.e., ground plane separation). For this modeling, the impedance looking toward the ground plane is purely inductive and equal to $Z_g = j\eta_0 \tan k_0 d_0$, where $k_0 = 2\pi/\lambda$ represents the wavenumber of the fundamental TEM mode in free space.

The above circuit model provides means to better understand the wideband performance of Munk's Current Sheet Array (CSA) [8]. Specifically, Munk added a capacitor between the dipole tips, which served to cancel the inductance from the GP. Thus, the input impedance seen by the dipole terminals is $Z_{in} = j\omega L + 1/j\omega C + Z_g/\eta_0$, where L is the dipole's self-inductance and C is the added capacitance. This intuitive addition of capacitance led to an impressive 4.5:1 impedance bandwidth (VSWR < 2). Notably, the array was only $\lambda/13$ thick at the lowest frequency of operation. Munk [8] also added a superstrate to improve the CSA dipole impedance bandwidth by as much as a factor of 2. Specifically, the impedance bandwidth of the array reached 9:1 [11].

Recently, Tzanidis *et al.* [10] proposed a conformal tightly coupled array (TCA) based on interwoven spiral elements as in Fig. 3. This new geometry provided 10:1 impedance bandwidth without a dielectric superstrate by introducing frequency-dependent capacitance via the interwoven spiral arms. As shown in Fig. 1, the spiral geometry involves intricate geometrical details, making it difficult to design and improve using full-wave analysis. Specifically, arm widths, gap dimensions, and interwoven arm lengths need be optimized to achieve wider impedance bandwidth. An equivalent circuit of the TCA spiral must therefore be developed for quick optimization of these parameters. This circuit model is discussed in what follows.

A challenge in developing the equivalent circuit for spirals is the modeling of the arms (standalone or interwoven). We chose

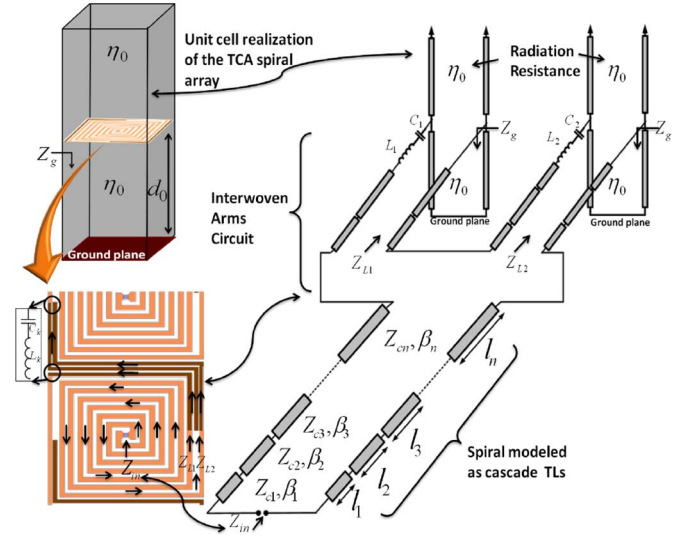


Fig. 3. Proposed equivalent circuit of the spiral array showing the spiral as cascade of TL sections and the interwoven arms as two TL in series terminated by lumped elements.

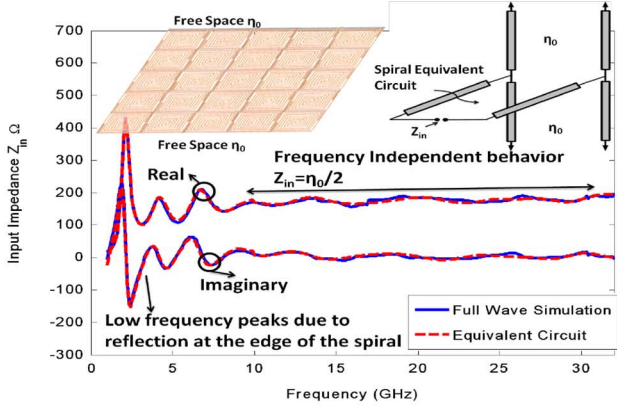
to model the spiral arms as TLs [12]. This choice assumes that only the fundamental two-wire transmission-line mode propagates along the spiral arms. As illustrated in Fig. 3, the spiral can be viewed as a cascade of ideal transmission line sections, terminated by an interwoven arm circuit and a radiation impedance Z_g/η_0 . To find the overall input impedance of the TCA array, we begin with the impedance of the spiral itself. We note that for the k th transmission line section, representing the spiral, the input impedance is given by [13]

$$Z_{in,k} = Z_{c,k} \frac{Z_{L,k} + jZ_{c,k} \tan(\beta_k l_k)}{Z_{c,k} + jZ_{L,k} \tan(\beta_k l_k)}. \quad (1)$$

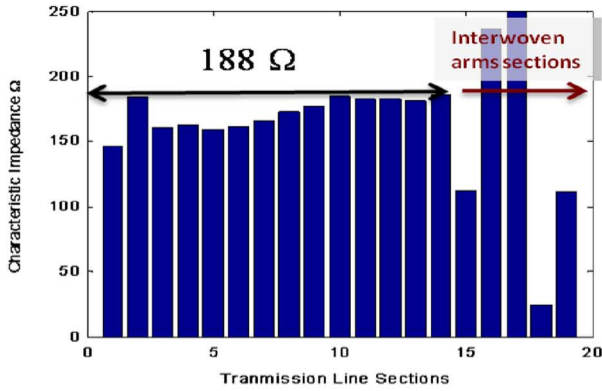
In this, $Z_{c,k}$ is the characteristic impedance of the k th TL section and $Z_{L,k}$ is the input impedance of the next TL section. Indeed, the TL section parameters $(Z_{L,k}, l_k)$ can be optimized to improve matching.

The interwoven spiral arms are critical to the wideband performance of the spiral array. However, its modeling within the equivalent circuit of Fig. 3 is challenging. Here, the interwoven arms are modeled using a pair of TLs in series. Both of them are terminated by an open circuit modeled as a lumped capacitor. A series inductor is also added to account for the edge coupling between adjacent interwoven arms. The characteristic impedance of these TL arms was selected after full-wave modeling of the interwoven arms. As seen from Fig. 4(a), the circuit model's overall impedance computation agrees well with full-wave analysis.

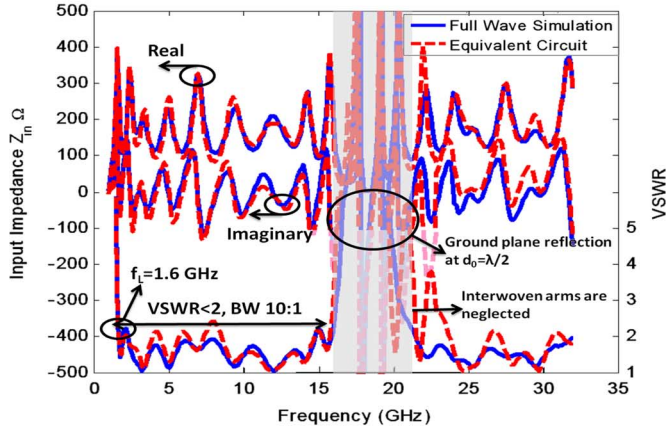
Curve fitting is performed to calculate the characteristic impedances of the spiral TL sections, as depicted in Fig. 4(b). The overall input impedance of the interwoven spiral, in presence of the GP backing, is given in Fig. 4(c). From this equivalent circuit model, the characteristic impedance of the spiral section is $\eta_0/2 = 188 \Omega$, especially near the spiral feed. As depicted in Fig. 4(a), the input impedance of the freestanding TCA achieves a frequency-independent behavior over a wide frequency band and becomes equal to $Z_{in} = 188 \Omega$. Here, the interwoven



(a)



(b)



(c)

Fig. 4. Input impedance comparison of the TCA consisting of interwoven spirals. (a) Freestanding array, (b) characteristic impedances calculated by curve fitting for use in the spiral circuit model, and (c) impedance in presence of the GP.

arms are not effective and can be neglected in the equivalent model. A simplified model can then be used consisting of a transmission line (spiral) terminated by the free-space radiation $Z_L = \eta_0/2 = 188 \Omega$. Plugging Z_{in} and Z_L in (1) and solving for Z_c , the characteristic impedance of the spiral sections (excluding the interwoven arms), should be about 188Ω to ensure matching. A comparison of the input impedance of the TCA spiral in presence of GP backing is given in Fig. 4(c). As seen, a 10:1 impedance bandwidth is obtained up to $f = 16$ GHz. However, when the GP is $\lambda/2$ thick at the frequency of operation, resonances appear. That is, at this frequency, the antenna

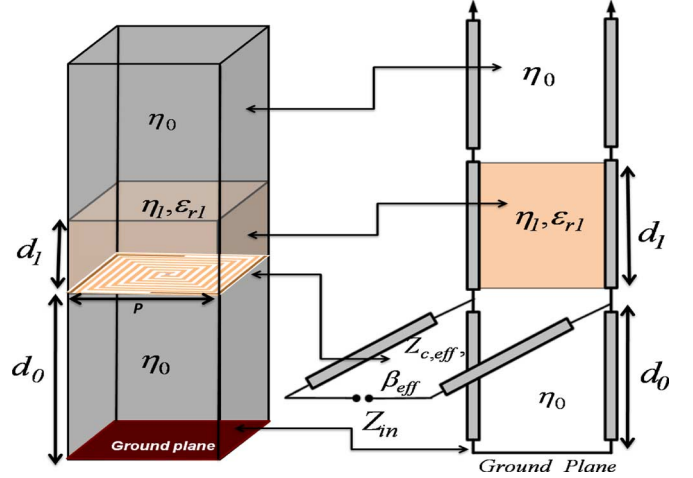


Fig. 5. Equivalent circuit of the tightly coupled spiral array with superstrate loading.

element with the ground plane behaves much like a resonant cavity. Both the circuit model and full-wave analysis predict these resonances.

III. DIELECTRIC SUPERSTRATE AND HIGHER-ORDER GRATING LOBES

We now proceed to employ the circuit model to improve the impedance bandwidth of the TCA even further. As already noted, adding a dielectric superstrate is a way to improve impedance bandwidth. Therefore, the circuit model of the TCA spiral needs to be modified as in Fig. 5. That is, the superstrate is modeled by introducing an additional TL using a characteristic impedance of $\eta_1 = 377 \Omega / \sqrt{\epsilon_{r1}}$. The length of the TL is, of course, equal to the thickness of the superstrate (d_1) as depicted in Fig. 5(a). However, the propagation constant and the characteristic impedance of the TL is not readily available. From [13], the effective permittivity is chosen to be $\epsilon_{eff} = (\epsilon_{r1} + 1)/2$. Therefore, the propagation constant of the wave traveling between the spiral arms must be $\beta_{keff} = \beta_k \sqrt{\epsilon_{eff}}$. The corresponding impedance is $Z_{c,keff} = Z_{c,k} / \sqrt{\epsilon_{eff}}$, where $Z_{c,k}$ is given in Fig. 4(b).

The circuit in Fig. 5 is used to optimize the superstrate permittivity (ϵ_{r1}) and thickness (d_1) to improve impedance bandwidth. Doing so, we find that for $\epsilon_r = 6$ and $d_1 = 7.5$ mm, the impedance bandwidth shifts down to 0.85 GHz as compared to 1.6 GHz when no superstrate is used [see Figs. 4(c) and 6]. This corresponds to a miniaturization factor of 1.9. Also, the achieved impedance bandwidth is 20:1 for a VSWR < 3 . As seen from Fig. 6 (shaded area), the addition of the superstrate triggers the onset of higher-order grating lobes due to trapped surface waves [14]. This occurs when the operational frequency is $f \geq nc/(P\sqrt{\epsilon_r}) = f_{c,n\epsilon_r}$, where n represents the mode, c is the free-space speed of light, and P stands for the array periodicity [see Fig. 5(a)]. Of course, in absence of a dielectric superstrate, the grating lobe emerges when $f \geq nc/P = f_{c,n}$. Therefore, the circuit model should be modified to account for the presence of higher-order modes. To do so, we need to compute the impedance of each mode.

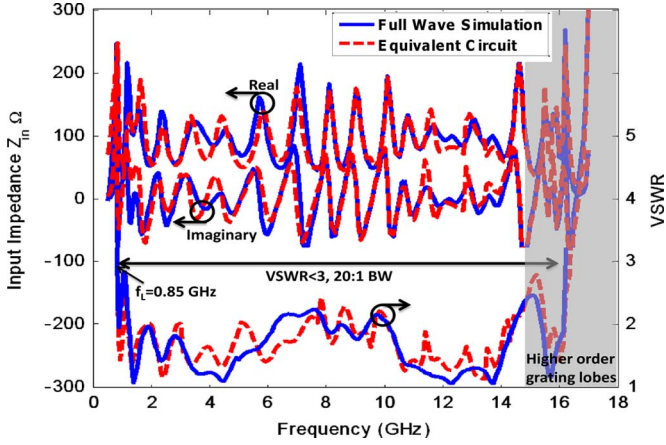


Fig. 6. Comparison of the input impedance for the array with superstrate: optimized TCA spiral as computed by the circuit model and full-wave simulations. Note that the VSWR < 3 impedance bandwidth is 20:1.

As depicted in Fig. 7, each higher-order mode can be modeled by a different TL, connected in parallel to the fundamental TL mode ($n = 0$). At broadside ($\theta = 0$), the propagation constant [15] and characteristic impedance of the n th mode are given by

$$\begin{aligned} k_{z,n\varepsilon_r} &= \sqrt{\varepsilon_r k_0^2 - \left(\frac{2n\pi}{P} + k_0^2 \sin^2\theta\right)^2} \\ &= j2\pi\sqrt{\varepsilon_r} / c\sqrt{|f^2 - f_{c,n\varepsilon_r}^2|} \\ &= j\beta_{z,n\varepsilon_r}, f < f_{c,n\varepsilon_r} \\ &= 2\pi\sqrt{\varepsilon_r} / c\sqrt{f^2 - f_{c,n\varepsilon_r}^2}, f \geq f_{c,n\varepsilon_r} \end{aligned} \quad (2)$$

$$\begin{aligned} \eta_{n\varepsilon_r} &= j\eta_0 / \sqrt{\varepsilon_r} \sqrt{|1 - (f_{c,n\varepsilon_r}/f)^2|} \\ &= jX_{n\varepsilon_r}, f < f_{c,n\varepsilon_r} \\ &= \eta_0 / \sqrt{\varepsilon_r} \sqrt{1 - (f_{c,n\varepsilon_r}/f)^2}, f \geq f_{c,n\varepsilon_r}. \end{aligned} \quad (3)$$

These can be used to compute the input impedance reflected by each TL representing the n th mode. We have

$$\begin{aligned} Z_{L,n} &= jX_{n\varepsilon_r} \frac{X_n - X_{n\varepsilon_r} \tanh(\beta_{z,n\varepsilon_r} d_1)}{X_{n\varepsilon_r} - X_n \tanh(\beta_{z,n\varepsilon_r} d_1)}, f < f_{c,n\varepsilon_r} \\ &= jX_{n\varepsilon_r} \frac{X_n + X_{n\varepsilon_r} \tan(k_{z,n\varepsilon_r} d_1)}{X_{n\varepsilon_r} - X_n \tan(k_{z,n\varepsilon_r} d_1)}, f_{c,n\varepsilon_r} < f < f_{c,n} \\ &= \eta_{n\varepsilon_r} \frac{\eta_n + j\eta_{n\varepsilon_r} \tan(k_{z,n\varepsilon_r} d_1)}{\eta_{n\varepsilon_r} + \eta_n \tan(k_{z,n\varepsilon_r} d_1)}, f > f_{c,n}. \end{aligned} \quad (4)$$

The overall impedance seen at the spiral feed is then determined by adding these impedances in parallel. However, we do note that $Z_{L,n}$ is reactive except for $n = 0$. That is, the $n \neq 0$ modes do not radiate and only contribute to the input impedance seen at the spiral terminals.

The input impedance of the overall TCA spiral with the optimized superstrate is given in Fig. 6. As seen (and in comparison to Fig. 4), the impedance bandwidth increased to 20:1 with VSWR < 3.

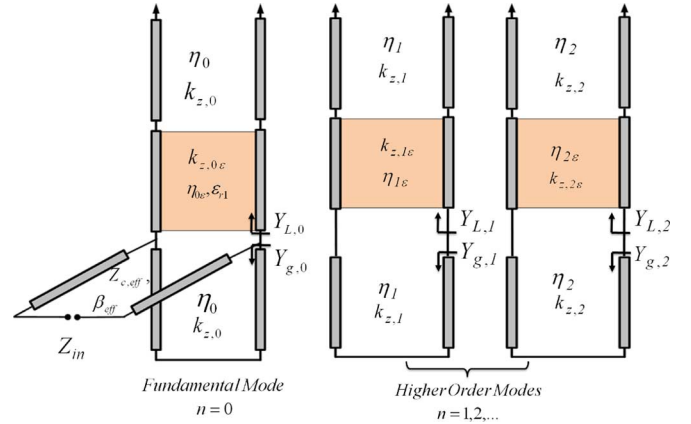


Fig. 7. Modified equivalent circuit taking into account the first two higher-order modes.

IV. CONCLUSION

An equivalent circuit model was developed for a tightly coupled spiral array. The model is based on representing the spiral array using sections of transmission lines of suitable characteristics. Optimization of the TL circuit parameters was then carried out to design the superstrate and achieve a 20:1 impedance bandwidth aperture.

REFERENCES

- [1] H. Holter, T.-H. Chio, and D. H. Schaubert, "Elimination of impedance anomalies in single- and dual-polarized endfire tapered-slot phased arrays," *IEEE Trans. Antennas Propag.*, vol. 48, no. 1, pp. 122–124, Jan. 2000.
- [2] M. Elsallal and J. Mather, "An ultra-thin, decade (10:1) bandwidth, modular "BAVA" array with low cross-polarization," in *Proc. IEEE APSURSI*, Jul. 2011, pp. 1980–1983.
- [3] J. Herd and P. Kao, "Broadband tem horn array for fopen radar," in *Proc. IEEE APSURSI*, Oct. 2002, pp. 452–455.
- [4] J. J. Lee, S. Livingstone, and R. Koenig, "A low-profile wide-band (5:1) dual-pol array," *IEEE Antennas Wireless Propag. Lett.*, vol. 2, pp. 46–49, 2003.
- [5] H. Wheeler, "The radiation resistance of an antenna in an infinite array or waveguide," *Proc. IRE*, vol. 36, no. 4, pp. 478–487, Apr. 1948.
- [6] C. Baum, "Transient arrays," *Ultra-Wideband, Short-Pulse Electromagn.*, vol. 3, pp. 129–138, 1997.
- [7] A. Neto and J. J. Lee, "Ultrawide-band properties of long slot arrays," *IEEE Trans. Antennas Propag.*, vol. 54, no. 2, pp. 534–543, Feb. 2006.
- [8] B. A. Munk, *Finite Antenna Arrays and FSS*. New York: Wiley, 2003.
- [9] P. Friederich, "A new class of broadband planar apertures," in *Proc. Allerton Antenna Appl. Symp.*, Sep. 2001, pp. 561–587.
- [10] I. Tzanidis, K. Sertel, and J. Volakis, "Interwoven spiral array (ISPA) with a 10:1 bandwidth on a ground plane," *IEEE Antennas Wireless Propag. Lett.*, vol. 10, pp. 115–118, 2011.
- [11] M. Jones and J. Rawnick, "A new approach to broadband array design using tightly coupled elements," in *Proc. IEEE MILCOM*, Orlando, FL, Oct. 2007, pp. 1–7.
- [12] J. L. Volakis, *Antenna Engineering Handbook*, 4th ed. New York: McGraw Hill, 2007.
- [13] D. Pozar, *Microwave Engineering*. New York: Wiley, 2005.
- [14] B. A. Munk, *Frequency Selective Surfaces: Theory and Design*. New York: Wiley, 2000.
- [15] G. Farrell and D. Kuhn, "Mutual coupling in infinite planar arrays of rectangular waveguide horns," *IEEE Trans. Antennas Propag.*, vol. AP-16, no. 4, pp. 405–414, Jul. 1968.